On-Orbit Demonstration of Range-Only Navigation for Small Satellite Formations

Ibrahima Sory Sow
Mechanical Engineering Department
Carnegie Mellon University
Pittsburgh, PA 15213
isow@andrew.cmu.edu

Max Holliday
Axient/MEIS
NASA Ames Research Center
Moffett Field, CA 94035
maximillian.a.holliday@nasa.gov

Jan Stupl
Small Spacecraft Technology Program
NASA Ames Research Center
Moffett Field, CA 94035
jan.stupl@nasa.gov

Roger Hunter
Small Spacecraft Technology Program
NASA Ames Research Center
Moffett Field, CA 94035
roger.c.hunter@nasa.gov

Zachary Manchester
Robotics Institute
Carnegie Mellon University
Pittsburgh, PA 15213
zacm@cmu.edu

Abstract—The availability of low-cost small satellites and commercial launch services has enabled a proliferation of distributed small-satellite missions. However, these missions require precise relative navigation, traditionally provided by expensive GNSS receivers that are limited to operation in low-Earth orbit. In this paper, we introduce a novel, scalable, cost-effective navigation method for both absolute and relative orbit determination that is suitable for resource-constrained small-satellite formations. Our approach combines inter-satellite ranging, a single "anchor" satellite with global measurements, and a highly accurate dynamics model in a nonlinear least-squares estimator. We demonstrate that our estimator can resolve the full orbital states of all spacecraft in a formation despite the inherent ambiguities of range-only navigation. We evaluate our method through numerical experiments with varied network topologies and an on-orbit demonstration during the PY4 satellite mission, achieving absolute positioning accuracy of 0.21m for the anchor satellite and 0.33m for the non-anchor satellite.

TABLE OF CONTENTS

1. INTRODUCTION

The increasing availability of low-cost commercial launch ride-share services has fueled the rapid proliferation of small satellite platforms, such as CubeSats. Missions involving fleets of multiple spacecraft acting as distributed sensing platforms [1] have gained significant interest due to their potential to achieve mission objectives at much lower costs than traditional, bulky, and expensive spacecraft. These applications span a wide range of fields, including continuous Earth monitoring [2,3], communication services [4], large baselines
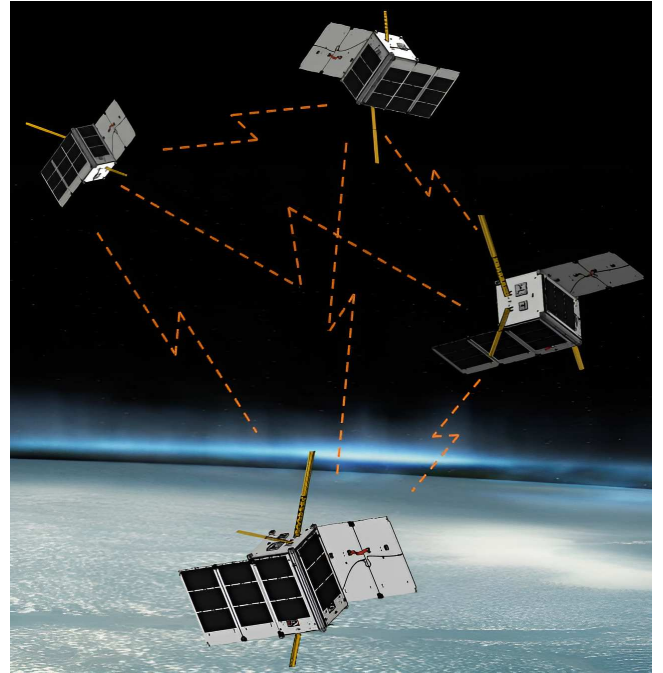
Figure 1. Four 1.5U CubeSats were deployed into a sun-synchronous orbit for the PY4 mission on March 4, 2024 to demonstrate precise inter-satellite ranging and relative orbit determination. Our maximum-likelihood estimation achieved sub-meter accuracy in locating spacecraft ranging with each other.

for high-resolution radio and optical astronomy [5, 6], and distributed in-situ measurements of the ionosphere and solar wind [7, 8].

However, the success of these missions depends critically on accurate navigation, which currently requires highly specialized hardware. Global Navigation Satellite Systems (GNSS) receivers (e.g., GPS) are commonly used for precise orbit determination [9, 10]. Yet, significant power constraints and potential radio frequency interference limit their continuous use in orbit, resulting in sparse data for navigation. Moreover, these receivers are expensive and subject to regulatory restrictions. To address these challenges, this paper presents a cost-effective and accessible method for absolute and relative orbit determination that is scalable to resource-constrained satellite formations.

The on-orbit relative navigation problem mirrors terrestrial *sensor network localization* [11, 12], where the absolute positions of each node (i.e., satellite) must be determined from partial inter-node measurements. Two-way ranging provides a low-cost method for distance measurements between each satellite in the formation. However, unlike bearing-only measurements that have a well-known range ambiguity [13], ranging alone leads to unobservability in three-dimensional space, as an infinite number of solutions exist for a single range measurement.

This paper presents an optimization-based navigation method to address the on-orbit relative and absolute navigation problem for a satellite formation, using only range measurements between satellites, a single "anchor" satellite with global-frame measurements, and high-accuracy orbital dynamics models. We evaluate the estimator through numerical experiments and an on-orbit demonstration using data from the ongoing PY4 mission [14]. This paper makes the following contributions:

1. An optimization-based batch estimator that fuses range and anchor measurements, jointly smoothing and determining the full relative and absolute orbital states of all spacecraft in a formation.
2. Numerical experiments comparing the performance of star and mesh formation topologies for both short- and long-range formations.
3. On-orbit performance evaluation with data from the PY4 satellites, demonstrating the estimator's robustness on low-cost hardware with intermittent anchor measurements.

The paper proceeds as follows: Section 2 reviews prior work on sensor-network localization and orbit determination. In Section 3, we detail our dynamics and measurement models. Section 4 introduces the optimization-based batch estimator, while Section 5 presents a covariance analysis. Section 6 then details several numerical experiments across different scenarios. Section 7 showcases the on-orbit experimental results from the PY4 mission. Finally, Section 8 summarizes our conclusions.

2. RELATED WORKS

In this section, we briefly survey previous research efforts addressing the problem of sensor-network localization and navigation for spacecraft formations.

Sensor-Network Localization

Sensor-network localization is well explored and categorized based on the type of relative measurements used [15]. The first category combines bearing and range information or uses relative full-state measurements, simplifying the estimation to a linear least squares problem. The second, known as the *range localization problem*, spans several decades of exploration and relies solely on distance measurements between neighboring nodes. However, solving this nonconvex optimization problem is NP-hard [16]. Eren et al. [17] showed that a network has a unique localization if the underlying graph is generically globally rigid. Hendrickson [18] proposed a distributed, graph-theoretic divide-and-conquer approach for the analogous molecule problem with perfect measurements. Calafiore et al. [12, 19] introduced a distributed gradient method to reduce the computational load in large networks. Other methods exploit optimization structure to relax the problem to semidefinite [20], sum-of-squares [21], or second-order cone [22] programs.

Localizing a network within a global frame requires knowledge of the absolute positions of a few nodes (anchors) in that frame. Without this, the network localization is not unique and is subject to arbitrary rotation and translation. While anchors are typically assumed, anchor-free methods [23] have been developed to address this ambiguity. Range-only localization also faces observability challenges, especially in 3D, where a single range measurement can yield infinite possible solutions. Shalaby et al. [24] proposed a framework incorporating inertial measurement unit (IMU) data and a two-tag system to provide attitude information with range measurements, ensuring instantaneous local observability. Cao et al. [25] used an extended Kalman filter (EKF) to fuse range and IMU data with a velocity model for a 2D robot, enhancing system observability.

Range-Only Spacecraft Navigation

Satellite relative navigation has often relied on "angles-only" or bearing measurements [26, 27]. Radiometric ranging with omnidirectional antennas is appealing for small satellites due to its simple implementation on low-cost hardware. Christian [28] studied observability properties using linear relative dynamics and found multiple trajectory solutions (2, 4, 8, or infinite) for the range-only navigation problem depending on the trajectory characteristics. Mirror solutions produce identical time histories of range measurements, making it impossible to distinguish between multiple possible valid solutions in the linear setting. Turan et al. [29] showed that in highly observable orbital configurations, less precise measurements can be effective, while high-frequency ranging can surprisingly degrade estimator performance. Additionally, they found that a mesh topology provides better state estimates than a centralized one. It is worth noting that range measurements lack bearing information; satellites can rotate arbitrarily while maintaining their inter-distance range. With only range measurements, our work leverages the nonlinearities in the dynamics model to guide the estimation process.

3. SYSTEM MODELING

We model a formation as a group of passive (unactuated) satellites orbiting Earth. The satellite that receives measurements relative to the global reference frame (e.g., GPS data, ground tracking) is termed the *chief* or *anchor* satellite, while the others are referred to as *deputy* satellites. The state of each satellite is represented in the Earth-centered inertial (ECI) frame by a cartesian 6-element state vector:

$$x = \begin{bmatrix} p \\ v \end{bmatrix} \tag{1}$$

where $p \in \mathbb{R}^3$ and $v \in \mathbb{R}^3$ denote the position and velocity vectors in the ECI frame, respectively. Equivalently, the satellite's state can also be described by the classical orbital elements [30]

$$x = \begin{bmatrix} a \\ e \\ i \\ \Omega \\ \omega \\ M \end{bmatrix} \tag{2}$$

where a is the semi-major axis, e is the eccentricity, i is the inclination, Ω is the longitude of the ascending node (RAAN), ω is the argument of perigee, and M is the true anomaly [30].

Figure 2. The four PY4 satellites, a collaboration between Carnegie Mellon University and NASA Ames Research Center, were launched on March 4, 2024 on the SpaceX Transporter 10 mission and deployed on a sun-synchronous orbit. The 1.5U satellites demonstrated a suite of novel navigation and control algorithms for low-cost platforms [14].

The motion of a spacecraft in Earth's orbit is typically approximated by the two-body dynamical model, where the only force considered is the central gravitational force exerted by Earth. This model assumes that Earth's mass distribution is spherically symmetric. However, this idealization neglects perturbing accelerations that introduce significant propagation errors over time [31]. These perturbations include Earth's non-uniform gravitational field, atmospheric drag, the gravitational influences of the Moon and Sun, and solar radiation pressure. In this work, we focus on formations in low Earth orbit (LEO) and model the two largest perturbations — Earth's non-spherical gravity a_g and atmospheric drag a_D [32]:

$$a_{sat} = a_g + a_D. \tag{3}$$

The continuous dynamics equations based on Eq. (3) are integrated to yield discrete-time dynamics using a fourth-order Runge-Kutta integrator,

$$x_{k+1} = f_{dyn}(x_k) + w_k, \tag{4}$$

where k is a time step, f is the resulting dynamics propagation function, and w_k is additive noise assumed to be drawn from a multivariate normal distribution with zero mean and covariance Q.

Gravity Model

The gravitational force is conservative and can be derived from a spherical-harmonic geopotential model U,

$$U = \frac{GM_\oplus}{\|p\|} \sum_{n=0}^{\infty} \sum_{m=0}^{n} \frac{R_\oplus^n}{\|p\|^n} P_{nm}(sin\phi)(C_{nm}cos(m\lambda) \tag{5}$$
$$+ S_{nm}sin(m\lambda)),$$
$$a_g = \nabla U, \tag{6}$$

where G is the gravitational constant, $M_\oplus$ is the mass of Earth, ϕ and λ are the latitude and longitude of the spacecraft, C_{nm} and S_{nm} are geopotential coefficients obtained from the EGM2008 model [33], and P_{nm} is the associated Legendre polynomial of degree n and order m [32].

Atmospheric Drag

Atmospheric drag accelerations represent the largest non-gravitational perturbations in LEO and act in the opposite direction of the spacecraft velocity,

$$a_D = -\frac{1}{2}C_D A\rho\|v_{rel}\|v_{rel}, \tag{7}$$

where C_D is the dimensionless drag coefficient, ρ is the atmospheric density, A is the cross-sectional area perpendicular to the velocity vector, and v_{rel} is the velocity relative to the atmosphere,

$$v_{rel} = v - \Theta \times p, \tag{8}$$

where Θ is the Earth's axial rotation.

Accurate predictions of the drag force are challenging due to the variable nature of atmospheric density (which can fluctuate by several orders of magnitude over an orbit due to altitude, weather, and solar activity), interactions between atmospheric particles and surface materials, and the varying attitude of the spacecraft. In practical settings, parameters in Eq.(7), such as ρ, are often estimated online, either directly or using a multiplicative relative parameterization [34].

Global-Frame Measurements

The chief satellite receives absolute full-state measurements (e.g. GPS, ground tracking) that can be intermittent,

$$y_k^{eci} = g_{eci}(x_k) = x_k + v_k, \tag{9}$$

where v_k is additive noise assumed to be drawn from a normal distribution with zero mean and variance R_v.

Ranging Models

Two-way ranging measurements between satellite i and j can be modeled as the norm of the difference between their positions p^i and p^j,

$$y_k^r = g_{range}(x_k^i, x_k^j) = \|p_k^i - p_k^j\| + w_k, \tag{10}$$

where w_k is additive noise assumed to be drawn from a normal distribution with zero mean and variance R_w.

A formation of satellites can collect ranging measurements in either a star (centralized) or mesh (distributed) configuration as illustrated in Fig. 3. In the star configuration, range measurements are taken between the chief satellite and each deputy, whereas the mesh configuration allows each satellite to range with multiple others.

4. OPTIMIZATION-BASED ESTIMATOR

Given the observability issues encountered when one tries to reconstruct the full relative states of the deputy spacecraft
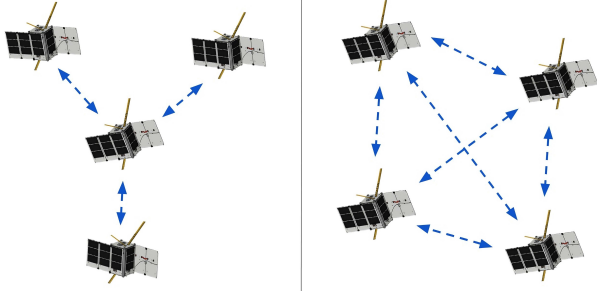
Figure 3. In the star configuration (left), the anchor satellite performs ranging with all other satellites exclusively. In the mesh configuration (right), all satellites communicate with each other.

based solely on range measurements (see Sec. 2), we include the absolute measurements of the anchor satellite as part of the estimation problem. In practice, those measurements (e.g. GPS) can be pre-filtered or smoothed, or combined with the ranging measurements in the estimation problem. We leverage the perturbations in our orbital-dynamics model to break the symmetry of the problem and resulting unobservability encountered in prior range-only spacecraft localization studies (see Sec. 2).

Traditionally, recursive Bayesian state-estimation techniques like the Kalman filter [35] and its many extensions are widely used for recovering full-state estimates given limited sensor measurements [36]. However, in situations where the dynamics are highly nonlinear and measurements are sparse, a nonlinear batch optimization technique can perform better. Batch methods formulate the state estimation problem as an optimization problem that recovers the maximum a-posteriori (MAP) estimate of the state history given a history of measurements. The nonlinear optimization problem takes the generic form,

$$\underset{z}{\text{minimize}} \quad \frac{1}{2}r(z,y)^T r(z,y)$$
$$\text{subject to} \quad c(z) = 0, \tag{11}$$

where z is the vector of decision variables, y is the vector of measurements, r is a residual function, and c specifies equality constraints. Nonlinear programming solvers, such as IPOPT [37] and SNOPT [38], can be used to solve such problems.

Because of the high fidelity of our dynamics model, we enforce the satellites' dynamics as hard constraints c_{dyn}. Given the high uncertainty of the drag acceleration, we estimate a scalar α that scales the nominal atmospheric density from our model ρ_{model} to better fit the data:

$$\rho = \alpha \rho_{model}. \tag{12}$$

In addition, raw ranging results need to be calibrated to account for hardware imperfections like delays and clock offsets. An affine calibration model can be fitted to the measurements y_{raw} and included in the optimization problem,

$$y_{calib} = a y_{raw} + b \tag{13}$$

where a and b are the affine parameters to be estimated.

We can then formulate the batch least-squares problem as,

$$\underset{x_{1:N}, \alpha, a, b}{\text{minimize}} \quad \frac{1}{2}r(x,y,a,b)^T W r(x,y,a,b)$$
$$\text{subject to} \quad c_{dyn}(x^a, \alpha) = 0, \tag{14}$$
$$c_{dyn}(x^d) = 0,$$

where x is a stacked vector of all spacecraft states over the batch time window with x^a and x^d indicating, respectively, the anchor and any other deputy spacecraft and $W = R^{-1}$ is a weighting matrix. The residual r is defined as a stacked vector of measurement residuals:

$$r_k^{eci} = y_k^{eci} - g_{eci}(x^a) \tag{15}$$
$$r_k^r = y_k^r - g_{range}(x_k^a, x_k^d). \tag{16}$$

Given the long time scales involved, we leverage the well-defined sparse structure of the constraint Jacobians to speed up solve times during our experiments and subsequent analysis. Note that the optimization (14) is nonconvex and converges to the nearest local minimum from an initial guess, a problem that is exacerbated with the presence of mirror solutions (see Sec. 2). In this work, we use heuristics (see Sec. 6) to generate a good initial guess for a given scenario.

5. COVARIANCE ANALYSIS

To study the impact of measurement uncertainty on the estimator outputs, we can map the measurement covariance matrix R into a state covariance estimate P_x using the Jacobian matrix of the residual function, leveraging the implicit function theorem [39]. An implicit function has the form,

$$r(x,y) = 0, \tag{17}$$

where x is the known input vector and y is the unknown output vector. We can then apply the implicit function theorem:

$$r(x,y) = \frac{\partial r}{\partial x}\Delta x + \frac{\partial r}{\partial y}\Delta y = 0,$$
$$\Delta y = -(\frac{\partial r}{\partial y})^{-1}\frac{\partial r}{\partial x}\Delta x, \tag{18}$$
$$\Delta y = A\Delta x.$$

We then use the Jacobian A to propagate the input covariance R to an output covariance on the resulting 3D states:

$$P_x = ARA^T. \tag{19}$$

While this method is straightforward in standard least-squares settings, our constrained optimization formulation necessitates a few additional steps [40]. We apply (18) instead to the associated Lagrangian of the optimization problem,

$$\mathcal{L}(x,y,\lambda) = \frac{1}{2}r(x,y)^T r(x,y) + \lambda^T c(x), \tag{20}$$

where r is the residual function, x is the stacked satellite states over the batch horizon, y is a vector containing all measurements, λ is a vector of Lagrange multipliers, and $c(x)$ is the vector of equality constraints. The derivation follows

with the vector of stacked variables $z = [x^T \quad \lambda^T]^T$:

$$\mathcal{L}(z, y) = \frac{\partial \mathcal{L}}{\partial z} \Delta z + \frac{\partial \mathcal{L}}{\partial y} \Delta y = 0,$$

$$\Delta z = -\left(\frac{\partial \mathcal{L}}{\partial z}\right)^{-1} \frac{\partial \mathcal{L}}{\partial y} \Delta y, \qquad (21)$$

$$\Delta z = A \Delta y,$$

where the necessary Jacobian $\frac{\partial \mathcal{L}}{\partial z}$ is retrieved through the Karush–Kuhn–Tucker (KKT) matrix [41, 42]:

$$\frac{\partial \mathcal{L}}{\partial z} = \begin{bmatrix} \nabla_x^2 \mathcal{L}(x, \lambda) & \nabla c(x)^T \\ \nabla c(x) & 0 \end{bmatrix}. \qquad (22)$$

6. NUMERICAL EXPERIMENTS

We conducted numerical experiments to evaluate the performance of the estimator for both star and mesh topologies in two distinct scenarios (see Table 2) over one hour:

1. Post-deployment drift immediately following spacecraft deployment
2. Long-distance ranging

Optimization problems were solved using the IPOPT solver [37]. Ground truth data was generated with a fine discretization and a high-fidelity dynamics model that includes high-order gravity terms, atmospheric drag, third-body influences, and solar radiation pressure. The estimator dynamics follow the model described in Sec. 3, incorporating a 10th-order gravity model, atmospheric drag, and a 5-second timestep. Satellite parameters were set to a mass of 2 kg, a cross-sectional area of 0.1 m^2, and a drag coefficient C_D of 2. The measurement uncertainty 1σ were 1.5 m, 1.5 cm/s, and 0.5 m for, respectively, the GPS position, GPS velocity, and range (taken from the datasheet of our hardware in Sec. 7). We chose a measurement sampling period of 60 seconds to reflect the power constraints encountered by small satellites.

Post-Deployment Drift

When satellites are deployed sequentially with slightly different initial conditions, relative position and velocity drifts occur among them. To simulate realistic conditions for sequentially deployed satellites, we model a sun-synchronous orbit [43] and perturb the relative states of the deputy spacecraft using Gaussian distributions with covariances of 10 m and 0.1 m/s, leading to relative distances of 2–4 km after one hour. In such cases, the estimator can be initialized using anchor GPS measurements and dynamics propagation for all satellites.

Long-Distance Ranging

We simulate a scenario where the satellites have a significant initial separation distance ranging from 5 km to 25 km. These longer distances produce noticeable differences in orbital dynamics compared to the deployment case, thus making the problem more observable. However, they also make it difficult to initialize the nonlinear estimator without an efficient heuristic. We initialize the estimator by sampling orbital elements around the anchor GPS measurements, applying deviations in the semi-major axis, inclination, and eccentricity within the range defined by the first range measurement. Each sampled state is propagated, and the residual between the

predicted trajectory and range is computed. The initial state is selected by minimizing the average squared residuals of the candidate trajectories.
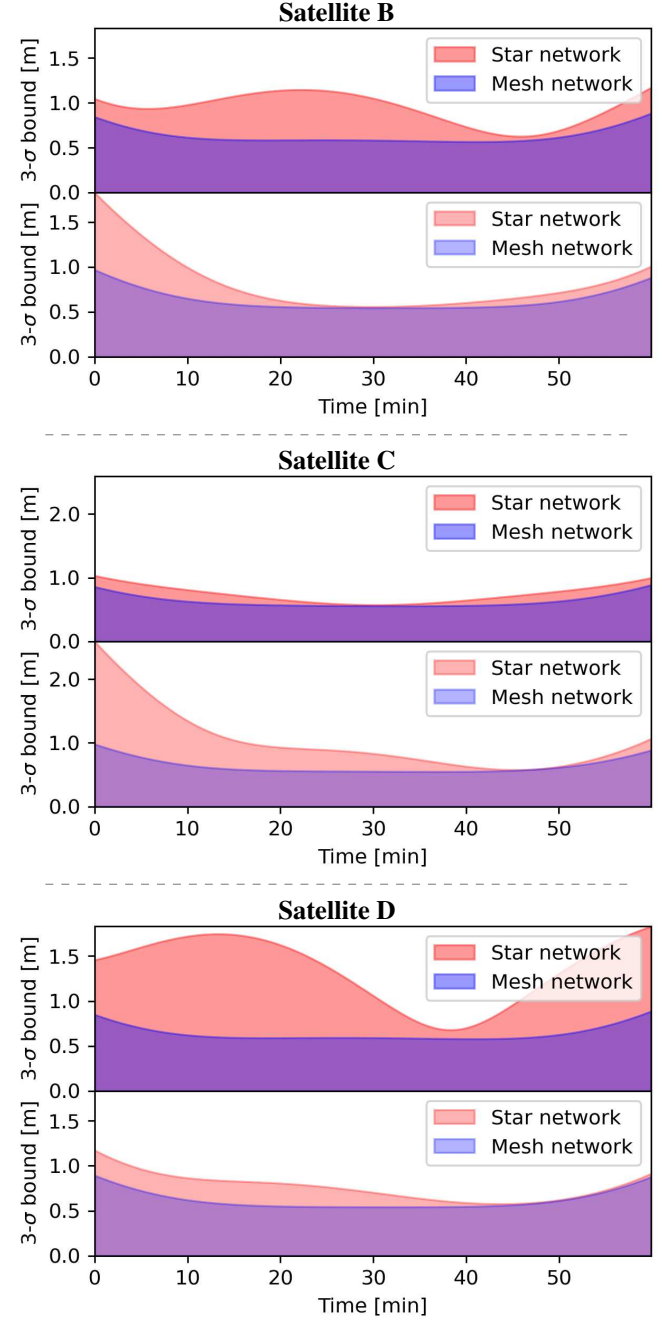
Results

Figure 4. 3-σ position deviation for the three simulated deputy satellites. For each satellite, the top figure corresponds to the post-deployment case, and the bottom one to the long-range case. The mesh configuration tends to reduce uncertainty compared to the star configuration.

Table 1 presents the absolute localization performance for the four-satellite formation in post-deployment and long-distance scenarios evaluated using star and mesh formation configurations. RMS position and velocity values are derived from the propagated state covariance matrix. Both scenarios show similar performance, demonstrating the robustness of

Table 1. Absolute localization errors for a four-satellite formation in post-deployment and long-distance scenarios with star and mesh configurations.

			Satellite A	Satellite B	Satellite C	Satellite D
Post-deployment	Star	RMS position [m]	0.2031	0.3168	0.2504	0.4634
		RMS velocity [m/s]	0.0002	0.0003	0.0002	0.0004
	Mesh	RMS position [m]	0.2031	0.2105	0.2110	0.2134
		RMS velocity [m/s]	0.0002	0.0002	0.0002	0.0002
Long-distance	Star	RMS position [m]	0.2030	0.2844	0.3683	0.2567
		RMS velocity [m/s]	0.0002	0.0003	0.0004	0.0002
	Mesh	RMS position [m]	0.2030	0.2124	0.2133	0.2072
		RMS velocity [m/s]	0.0002	0.0002	0.0002	0.0002

Table 2. Initial conditions of the anchor for the two simulated high-inclination sun-synchronous orbits.

Orbital elements	Post-deployment	Long distance
a	6995 km	6880 km
e	$1e^{-4}$	$6e^{-4}$
i	97.85°	97.41°
Ω	196.92°	269.76°
ω	148.25°	233.29°
M	225.43°	342.07°

Table 3. Relative localization accuracy for post-deployment (P) and long-distance (L) scenarios.

Mean RMS	Relative distance [m]	Relative velocity [m/s]
Star (P)	0.7170	0.0045
Mesh (P)	0.4943	0.0010
Star (L)	0.3585	0.0023
Mesh (L)	0.5004	0.0014

the estimator to range distances up to 30 km. The full mesh configuration consolidates RMS errors across all satellites, yielding around 0.2m and 0.0002 m/s for both scenarios. As expected, Satellite A, the anchor, achieves the best localization, while the mesh configuration effectively reduces errors for the other satellites to the anchor level.

For relative states, Table 3 shows an improvement in localization with the mesh formation. The positioning uncertainty (1σ) is approximately 0.01% of the maximum satellite range in the post-deployment star and mesh configurations and improving to around 0.001% in the other long-distance cases.

Figure 4 illustrates the covariance trajectory for the position of the non-anchor satellites B, C, and D over the time horizon in both scenarios. We can observe that the mesh configuration achieves a 1.5x to 3x reduction in uncertainty at close range, although this advantage diminishes slightly in the long-range scenario. Moreover, the star configuration exhibits significantly more variability in uncertainty throughout the trajectory, whereas the mesh configuration provides a more stable and uniform uncertainty across all states. This suggests that adding additional crosslinks between nodes offers a

robust strategy for reducing uncertainty, thereby enhancing localization performance.

7. ON-ORBIT DEMONSTRATION

The four 1.5U PY4 CubeSats, shown in Fig. 2, were deployed into an initial 515 km altitude circular sun-synchronous orbit at a 97.5° inclination on March 4, 2024, via the SpaceX Transporter 10 mission. One of the primary mission objectives was to demonstrate precise inter-satellite ranging and relative orbit determination [14].

Figure 5 shows a high-level depiction of the relevant onboard communication architecture. Two-way time-of-flight ranging was conducted using S-band Semtech SX1280 LoRa radio modules with a 0.5 W transmit power, utilizing LoRa chirp spread-spectrum modulation [44]. The SX1280 hardware-level ranging offers meter-level accuracy with proper calibration, making it a low-cost CubeSat navigation solution. Each satellite also carried a NovAtel OEM719 GPS receiver for ground-truth validation, with data precisely timestamped by the onboard GPS. The 1σ measurement uncertainties for the estimator is extracted from the datasheets of the GPS and radio: 1.5 m, 1.5 cm/s, and 0.5 m for, respectively, the GPS position, GPS velocity, and LoRa range measurements.
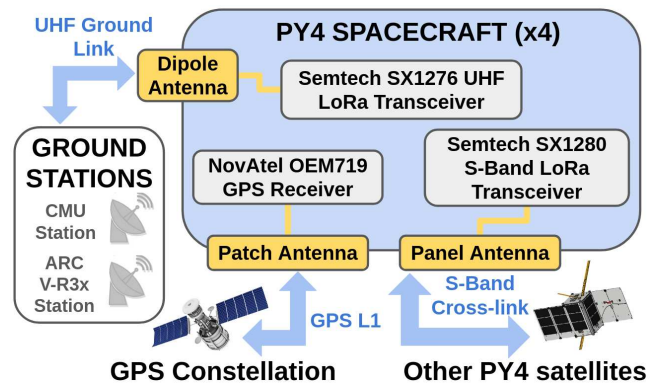

Figure 5. High-level radio architecture for the PY4 satellites. Each CubeSat carries a NovAtel OEM719 GPS receiver, Semtech SX1280 S-band LoRa radio module to perform cross-link communication and two-way time-of-flight ranging, and a Semtech SX1276 UHF LoRa radio module for ground communications [14].

Table 4. **On-orbit localization results for PY4-B and PY4-C, showing RMS values for the trajectory and the smallest (best) single-measurement error.**

	PY4-B	PY4-C
Absolute Position (RMS) [m]	0.2126	0.3305
Absolute Position (best) [m]	0.1892	0.2578
Absolute Velocity (RMS) [m/s]	0.0002	0.0003
Absolute Velocity (best) [m/s]	0.0001	0.0002
Relative Position (RMS) [m]		0.0138
Relative Position (best) [m]		0.0105
Relative Velocity (RMS) [m/s]		6.58×10^{-5}
Relative Velocity (best) [m/s]		9.0×10^{-6}

Figure 7. Estimated 3D spacecraft trajectory of PY4-C relative to PY4-B (blue) and individual range measurements (red) during the 64-min time window in the Local-Vertical-Local-Horizontal frame. The estimator achieved a relative positioning accuracy of 0.0138 m.

8. CONCLUSION

We presented a navigation method for relative and absolute orbit determination of a satellite formation using only range measurements and a single anchor satellite. A high-accuracy dynamics model enables a batch nonlinear least-squares estimator to address ambiguities inherent in range-only navigation. Numerical experiments with star and mesh configurations demonstrated that the additional measurements from a mesh approach can increase the robustness and accuracy of estimates. Our on-orbit experiments with the PY4 satellites validated our method on low-cost hardware with intermittent anchor measurements.

A major limitation of our method is the inherent nonconvexity of the estimation problem, making the solution dependent on solver initialization. While on-the-ground processing can rely on expert tuning and heuristics, convergence to mirror solutions from poor initializations could still present problems for deployment in a fully autonomous on-orbit scenario.

Much room for future work on range-based satellite navigation remains: First, we plan to perform an in-depth observability analysis that accounts for drag and higher-order gravity perturbations in the dynamics, as well as spacecraft formation geometry. Second, we will systematize the initialization heuristics used in this work in an effort to build a fully autonomous system suitable for on-orbit deployment.
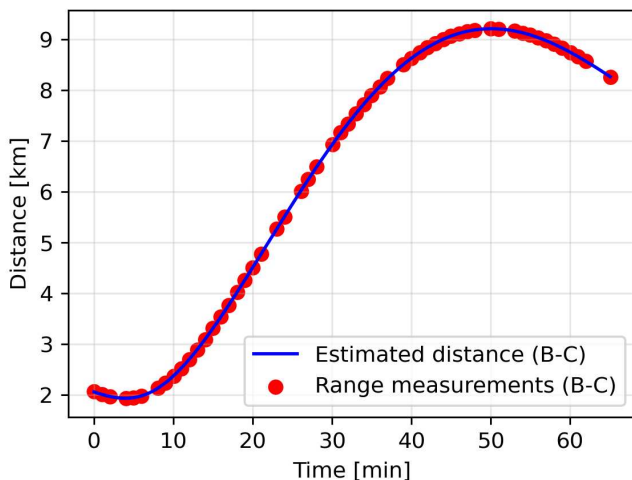
Figure 6. Estimated inter-satellite range (blue) and individual range measurements (red) showing close agreement. The raw range measurements were calibrated with an affine model.

Ranging measurements were collected between PY4-B (anchor) and PY4-C (deputy) over a 64-minute period. After downlink, the dataset was post-processed and time-synchronized before input to the estimator. The spacecraft performed ranging measurements every 60 seconds. Unlike the simulations in Sec. 6, GPS positions were relatively sparse and variable (period ranging from 1 to 3 minutes). Despite this, the estimator managed to achieve sub-meter accuracy for both spacecraft, as shown in Table 4. As expected, PY4-B is better-localized given its anchor status. Note that the simulated results in Sec. 6 did not include a range calibration model or atmospheric drag estimation, explaining the improved performance in the on-orbit experiments.

Figure 6 shows the estimated inter-satellite range (blue) closely matching the calibrated range measurements (red). Figure 7 illustrates the 3D trajectory of PY4-C relative to PY4-B with the individual range measurements in the Local-Vertical-Local-Horizontal (LVLH) frame. We note that PY-4C exhibited significant drift in the along-track direction.
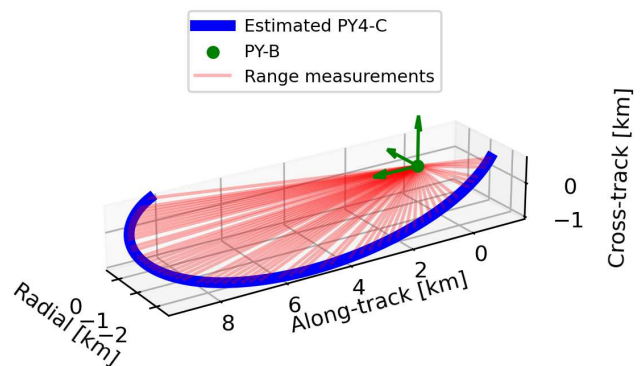
REFERENCES

[1] B. Lucia, B. Denby, Z. Manchester, H. Desai, E. Ruppel, and A. Colin, "Computational Nanosatellite Constellations: Opportunities and Challenges," *GetMobile: Mobile Comp. and Comm.*, vol. 25, no. 1, pp. 16–23, Jun. 2021.

[2] C. Foster, H. Hallam, and J. Mason, "Orbit Determination and Differential-drag Control of Planet Labs Cubesat Constellations," Sep. 2015. [Online].

Available: http://arxiv.org/abs/1509.03270

[3] C. Foster, J. Mason, V. Vittaldev, L. Leung, V. Beuke-laers, L. Stepan, and R. Zimmerman, "Constellation Phasing with Differential Drag on Planet Labs Satellites," *Journal of Spacecraft and Rockets*, vol. 55, no. 2, pp. 473–483, 2018.

[4] N. Saeed, A. Elzanaty, H. Almorad, H. Dahrouj, T. Y. Al-Naffouri, and M.-S. Alouini, "CubeSat Communications: Recent Advances and Future Challenges," *IEEE Communications Surveys & Tutorials*, vol. 22, no. 3, pp. 1839–1862, 2020.

[5] S. Engelen, C. J. M. Verhoeven, and M. J. Bentum, "Olfar, A Radio Telescope Based on Nano-Satellites in Moon Orbit," *Small Satellite Conference*, Aug. 2010. [Online]. Available: https://digitalcommons.usu.edu/smallsat/2010/all2010/20

[6] S. Wu, W. Chen, Y. Zhang, W. Baan, and T. An, "SULFRO: a Swarm of Nano-/Micro-Satellite at SE L2 for Space Ultra-Low Frequency Radio Observatory," *Small Satellite Conference*, Aug. 2014. [Online]. Available: https://digitalcommons.usu.edu/smallsat/2014/AdvTechI/8

[7] F. Alibay, J. C. Kasper, T. J. W. Lazio, and T. Neilsen, "Sun radio interferometer space experiment (SunRISE): Tracking particle acceleration and transport in the inner heliosphere," in *2017 IEEE Aerospace Conference*, Mar. 2017, pp. 1–15.

[8] L. Policastri and J. Woodburn, "HELIOSWARM: SPACE-BASED RELATIVE RANGING FOR A CUBESAT CLUSTER MISSION IN A 2:1 LUNAR RESONANT ORBIT," Aug. 2019.

[9] S. D'Amico, "Autonomous formation flying in low earth orbit," Ph.D. dissertation, Technical University of Delft, 01 2010.

[10] Y. Lou, X. Dai, X. Gong, C. Li, Y. Qing, Y. Liu, Y. Peng, and S. Gu, "A review of real-time multi-GNSS precise orbit determination based on the filter method," *Satellite Navigation*, vol. 3, no. 1, p. 15, Jul. 2022. [Online]. Available: https://doi.org/10.1186/s43020-022-00075-1

[11] G. Mao, B. Fidan, and B. D. O. Anderson, "Wireless sensor network localization techniques," *Computer Networks*, vol. 51, no. 10, pp. 2529–2553, Jul. 2007.

[12] G. C. Calafiore, L. Carlone, and M. Wei, "A Distributed Technique for Localization of Agent Formations From Relative Range Measurements," *IEEE Transactions on Systems, Man, and Cybernetics - Part A: Systems and Humans*, vol. 42, no. 5, pp. 1065–1076, Sep. 2012.

[13] A. W. Koenig and S. D'Amico, "Observability-aware numerical algorithm for angles-only initial relative orbit determination," in *2020 AAS/AIAA Astrodynamics Specialist Conference*, 2020.

[14] M. Holliday, R. Ticknor, J. Stupl, R. Hunter, P. Fisch, I. Sow, J. Willis, and Z. Manchester, "The PY4 Mission: A Low-Cost Demonstration of CubeSat Formation-Flying Technologies," *Small Satellite Conference*, Aug. 2024.

[15] G. C. Calafiore, L. Carlone, and M. Wei, "Position estimation from relative distance measurements in multi-agents formations," in *18th Mediterranean Conference on Control and Automation, MED'10*, Jun. 2010, pp. 148–153.

[16] J. Aspnes, T. Eren, D. K. Goldenberg, A. S. Morse, W. Whiteley, Y. R. Yang, B. D. O. Anderson, and P. N. Belhumeur, "A Theory of Network Localization," *IEEE Transactions on Mobile Computing*, vol. 5, no. 12, pp. 1663–1678, Dec. 2006.

[17] T. Eren, O. Goldenberg, W. Whiteley, Y. Yang, A. Morse, B. Anderson, and P. Belhumeur, "Rigidity, computation, and randomization in network localization," in *IEEE INFOCOM 2004*, vol. 4, Mar. 2004, pp. 2673–2684 vol.4.

[18] B. Hendrickson, "The Molecule Problem: Exploiting Structure in Global Optimization," *SIAM Journal on Optimization*, vol. 5, no. 4, pp. 835–857, Nov. 1995.

[19] G. C. Calafiore, L. Carlone, and M. Wei, "A distributed gradient method for localization of formations using relative range measurements," in *2010 IEEE International Symposium on Computer-Aided Control System Design*, Sep. 2010, pp. 1146–1151.

[20] P. Biswas and Y. Ye, "Semidefinite programming for ad hoc wireless sensor network localization," in *Third International Symposium on Information Processing in Sensor Networks, 2004. IPSN 2004*, Apr. 2004, pp. 46–54.

[21] J. Nie, "Sum of squares method for sensor network localization," *Computational Optimization and Applications*, vol. 43, no. 2, pp. 151–179, Jun. 2009.

[22] P. Tseng, "Second-Order Cone Programming Relaxation of Sensor Network Localization," *SIAM Journal on Optimization*, vol. 18, no. 1, pp. 156–185, Jan. 2007.

[23] N. B. Priyantha, H. Balakrishnan, E. Demaine, and S. Teller, "Anchor-free Distributed Localization in Sensor Networks," Apr. 2003.

[24] M. Shalaby, C. C. Cossette, J. R. Forbes, and J. Le Ny, "Relative Position Estimation in Multi-Agent Systems Using Attitude-Coupled Range Measurements," *IEEE Robotics and Automation Letters*, vol. 6, no. 3, pp. 4955–4961, Jul. 2021.

[25] Y. Cao, C. Yang, R. Li, A. Knoll, and G. Beltrame, "Accurate position tracking with a single UWB anchor," *2020 IEEE International Conference on Robotics and Automation (ICRA)*, pp. 2344–2350, May 2020.

[26] D. C. Woffinden and D. K. Geller, "Observability Criteria for Angles-Only Navigation," *IEEE Transactions on Aerospace and Electronic Systems*, vol. 45, no. 3, pp. 1194–1208, Jul. 2009.

[27] D. K. Geller and A. Perez, "Initial Relative Orbit Determination for Close-in Proximity Operations," *Journal of Guidance, Control, and Dynamics*, vol. 38, no. 9, pp. 1833–1842, 2015.

[28] J. A. Christian, "Relative Navigation Using Only Inter-satellite Range Measurements," *Journal of Spacecraft and Rockets*, vol. 54, no. 1, pp. 13–28, 2017.

[29] E. Turan, S. Speretta, and E. Gill, "Performance analysis of crosslink radiometric measurement based autonomous orbit determination for cislunar small satellite formations," *Advances in Space Research*, vol. 72, no. 7, pp. 2710–2732, Oct. 2023.

[30] K. T. Alfriend, *Spacecraft formation flying dynamics, control and navigation*, ser. Elsevier astrodynamics series. Amsterdam ;: Elsevier/Butterworth-Heinemann, 2010.

[31] J. E. Prussing and B. A. Conway, *Orbital Mechanics*, 2nd ed. New York: Oxford University Press, 2013.

[32] O. Montenbruck and E. Gill, *Satellite Orbits: Models, Methods and Applications*. Springer Science & Business Media, Dec. 2012.

[33] N. K. Pavlis, S. A. Holmes, S. C. Kenyon, and J. K. Factor, "The development and evaluation of the Earth Gravitational Model 2008 (EGM2008)," *Journal of Geophysical Research: Solid Earth*, vol. 117, no. B4, 2012.

[34] K. S. Tracy, G. Falcone, and Z. Manchester, "Robust Entry Guidance with Atmospheric Adaptation," in *AIAA SCITECH 2023 Forum*, ser. AIAA SciTech Forum. American Institute of Aeronautics and Astronautics, Jan. 2023.

[35] R. E. Kalman, "A New Approach to Linear Filtering and Prediction Problems," *Journal of Basic Engineering*, vol. 82, no. 1, pp. 35–45, Mar. 1960.

[36] S. Thrun, W. Burgard, and D. Fox, *Probabilistic Robotics*. Cambridge, MA: MIT Press, 2005.

[37] A. Wächter and L. T. Biegler, "On the implementation of an interior-point filter line-search algorithm for large-scale nonlinear programming," *Mathematical Programming*, vol. 106, no. 1, pp. 25–57, Mar. 2006.

[38] P. E. Gill, W. Murray, and M. A. Saunders, "SNOPT: An SQP Algorithm for Large-Scale Constrained Optimization," *SIAM Journal on Optimization*, vol. 12, no. 4, pp. 979–1006, Jan. 2002.

[39] C. B. Allendoerfer, *Theorems about Differentiable Functions*. New York: Macmillan, 1974.

[40] B. Amos, I. D. J. Rodriguez, J. Sacks, B. Boots, and J. Z. Kolter, "Differentiable MPC for End-to-end Planning and Control," Oct. 2018. [Online]. Available: https://arxiv.org/abs/1810.13400v3

[41] S. Boyd and L. Vandenberghe, *Convex optimization*. Cambridge university press, 2004.

[42] J. Nocedal and S. J. Wright, *Numerical Optimization*, 2nd ed. New York, NY, USA: Springer, 2006.

[43] R. J. Boain, "A-B-Cs of sun-synchronous orbit mission design," Feb. 2004. [Online]. Available: https://ntrs.nasa.gov/citations/20210001902

[44] T. Janssen, N. BniLam, M. Aernouts, R. Berkvens, and M. Weyn, "LoRa 2.4 GHz Communication Link and Range," *Sensors*, vol. 20, no. 16, p. 4366, Jan. 2020.

BIOGRAPHY

Ibrahima Sory Sow *is a graduate student with the Robotic Exploration Lab at Carnegie Mellon University. He received his B.S. in Electromechanical Engineering from Université libre de Bruxelles in 2022. He is a Belgian American Educational Foundation Fellow. His research interests include optimization-based planning and control for robotic systems and spacecraft guidance, navigation, and control.*

Max Holliday *is a subject matter expert at NASA Ames Research Center specializing in small spacecraft electronic systems. He received his PhD in 2022 from Stanford University and his BS in 2014 from New Mexico Institute for Mining and Technology, both in materials science and engineering. Prior to NASA, he was principal investigator in the Remote Sensing Department at Sandia National Laboratories from 2014 to 2018.*

Jan Stupl *is a project manager in NASA's Small Spacecraft Technology Program. He is currently lead systems engineer for the CubeSat Laser Infrared CrosslinK (CLICK) mission and supports the Pathfinder Technology Demonstrator series of CubeSat missions. Jan received his PhD in physics from University of Hamburg and was a postdoc at the Center for International Security and Cooperation (CISAC) at Stanford University before joining NASA.*

Roger Hunter *currently serves as Program Manager for NASA's Small Spacecraft Technology Program. He holds academic degrees from the University of Georgia, The US Air Force Institute of Technology, and the US Air Force School of Advanced Airpower Studies, and he has over 45 years of experience in US Department of Defense, commercial, and government space missions.*

Zachary Manchester *is an assistant professor in the Robotics Institute at Carnegie Mellon University and director of the Robotic Exploration Lab. He received a PhD in aerospace engineering in 2015 and a BS in applied physics in 2009, both from Cornell University. He was a postdoctoral fellow at Harvard from 2015 to 2017 and an assistant professor at Stanford from 2018 to 2020. His research interests include numerical optimization, control, and estimation with applications to aerospace and robotic systems with challenging nonlinear dynamics.*